Articles

Crystal Structures of Cytochrome c_L and Methanol Dehydrogenase from *Hyphomicrobium denitrificans*: Structural and Mechanistic Insights into Interactions between the Two Proteins[†,‡]

Masaki Nojiri,*[,§] Daisuke Hira,[§] Kazuya Yamaguchi,[§] Toshihide Okajima,[||] Katsuyuki Tanizawa,[||] and Shinnichiro Suzuki[§]

Department of Chemistry, Graduate School of Science, Osaka University, Toyonaka, Osaka 560-0043, Japan, and The Institute of Scientific and Industrial Research, Osaka University, Ibaraki, Osaka 567-0047, Japan

Received September 15, 2005; Revised Manuscript Received January 13, 2006

ABSTRACT: Methanol dehydrogenase (*Hd*-MDH) and its physiological electron acceptor, cytochrome c_L (*Hd*-Cyt c_L), isolated from a methylotrophic denitrifying bacterium, *Hyphomicrobium denitrificans* A3151, have been kinetically and structurally characterized; the X-ray structures of *Hd*-MDH and *Hd*-Cyt c_L have been determined using molecular replacement at 2.5 and 2.0 Å resolution, respectively. To explain the mechanism for electron transfer between these proteins, the dependence of MDH activity on the concentration of *Hd*-Cyt c_L has been investigated at pH 4.5−7.0. The Michaelis constant for *Hd*-Cyt c_L shows the smallest value (∼0.3 μM) at pH 5.5. The pseudo-first-order rate constant (k_{obs}) of the reduction of *Hd*-Cyt c_L exhibits a hyperbolic concentration dependence of *Hd*-MDH at pH 5.5, although k_{obs} linearly increases at pH 6.5. These findings indicate formation of a transient complex between these proteins during an electron transfer event. *Hd*-MDH (148 kDa) is a large tetrameric protein with an $\alpha_2\beta_2$ subunit composition, showing a high degree of structural similarity with other MDHs. *Hd*-Cyt c_L (19 kDa) exhibiting the α-band at 550.7 nm has a unique C-terminal region involving a disulfide bond between Cys47 and Cys165. Moreover, there is a pair of *Hd*-Cyt c_L monomers related with a pseudo-2-fold axis of symmetry in the asymmetric unit, and the two monomers tightly interact with each other through three hydrogen bonds. This configuration is the first example in the studies of cytochrome *c* as the physiological electron acceptor for MDH. The docking simulation between the coupled *Hd*-Cyt c_L molecules and the heterotetrameric *Hd*-MDH molecule has been carried out.

Methanol dehydrogenase (MDH,[1] EC 1.1.99.8) is a pyrroloquinoline quinone (PQQ)-containing protein found in the periplasm of methylotrophic bacteria. The enzyme catalyzes the oxidation of methanol to formaldehyde and utilizes a specific cytochrome *c* as an electron acceptor (*1*−*5*). This methanol oxidation is the most important first step on energy transduction in methylotrophs, coupling to electron transport chains for ATP production driven by the proton-motive force across the inner cytoplasmic membrane (*4*, *5*). All of the known methylotrophic bacteria contain at least two soluble class I *c*-type cytochromes in the periplasmic space (*4*−*8*). One is basic cytochrome c_H (Cyt c_H, ca. 15 kDa), and the other is acidic cytochrome c_L (Cyt c_L, ca. 20 kDa). The reduced PQQ moiety of MDH, which accepts two electrons from methanol to produce formaldehyde, transfers two electrons one at a time to Cyt c_L, forming a semiquinone form after the first electron transfer (*9*, *10*). Cyt c_L is subsequently oxidized by Cyt c_H, which finally transfers electrons to cytochrome *c* oxidase (*5*, *11*).

$$CH_3OH \rightarrow MDH \rightarrow \text{Cyt } c_L \rightarrow \text{Cyt } c_H \rightarrow \text{oxidase} \rightarrow O_2$$

The reaction cycle of MDH with its electron acceptor, Cyt c_L, has been analyzed by steady-state and stopped-flow kinetic techniques and isotope effects using CD_3OH (*9*, *10*). From the stopped-flow experiments, it was concluded that Cyt c_L is an excellent oxidant of reduced MDH at pH 7, and not at pH 9. Under steady-state conditions, the overall turnover of the enzyme is slower at pH 9 than at pH 7, because the oxidation process of reduced MDH is a rate-limiting step at pH 9. The lack of a deuterium isotope effect using CD_3OH at pH 9 also indicated that a rate-limiting process is not substrate conversion, but the following electron transfer process from reduced MDH to Cyt c_L.

[†] This work was supported by a Grant-in-Aid for Scientific Research (16750144) from the Ministry of Education, Science, Sports and Culture of Japan (to M.N.), a Grant for Environmental Research Projects from the Sumitomo Fundation, and the 21st Century Center of Excellence Program "Creation of Integrated EcoChemistry" of Osaka University (to S.S.).

[‡] The coordinates have been deposited in the Protein Data Bank and are available as entries 2D0V (*Hd*-MDH) and 2D0W (*Hd*-Cyt c_L).

* To whom correspondence should be addressed. Fax: +81-6-6850-5785. E-mail: nojiri@ch.wani.osaka-u.ac.jp.

[§] Graduate School of Science.

[||] The Institute of Scientific and Industrial Research.

10.1021/bi051877j CCC: $33.50
Published on Web 02/22/2006

The electrostatic interaction between basic amino acid residues of MDH and acidic amino acid residues of Cyt c_L has been proposed (*12*, *13*). Moreover, it has been demonstrated that the interaction is strongly inhibited by low concentrations of salts and the extent of inhibition is directly related to the ionic strength of the medium (NaCl concentration). In addition, the hydrophobic interaction between these proteins also seems to be important, as indicated by the X-ray structure of MDH from *Methylobacterium extorquens* (*Me*-MDH) (*14*). PQQ is buried inside an internal chamber communicating with the exterior through a hydrophobic funnel in the protein surface, which is the site for interaction with Cyt c_L. The kinetic investigation of the interaction between the two proteins from *Paracoccus denitrificans* has led to a similar conclusion (*15*, *16*).

The MDHs from three bacteria, *M. extorquens* AM1 (*17*), *Methylophilus methylotrophus* W3A1 (*18*, *19*), and *Paracoccus denitrificans* (*20*, *21*), are $\alpha_2\beta_2$ heterotetramers with subunits of 62−65 kDa (α) and 8−9 kDa (β). These crystal structures show that the heterotetramer is composed of a pair of tightly associated $\alpha\beta$ subunits related by a pseudo-2-fold axis of symmetry. Each α subunit is an 8-fold β-propeller, and each propeller blade is a four-stranded antiparallel β-sheet. PQQ is located approximately on the pseudo-8-fold axis of symmetry of the β-propeller. The smaller β-subunit forms a mainly α-helical structure, which wraps around the outside of the α-subunit. Moreover, there are some remarkable structural features in the MDH structures such as a vicinal disulfide at the active center and a "tryptophan docking motif" in the β-propeller superbarrel.

The Cyt c_L from *M. extorquens* AM1 (*Me*-Cyt c_L), which is an electron acceptor for the cognate MDH (*Me*-MDH), is similar to class I cytochrome *c*, but its amino acid sequence shows that it constitutes a separate novel class of *c*-type cytochromes (*22*). Class I is the most abundant with molecules sharing the following features: a low-spin heme located near the N-terminus, a His-Met heme axial coordination site, and a polypeptide chain of 80−120 amino acids (*23*). The X-ray crystal structure of *Me*-Cyt c_L has been reported only in the Protein Data Bank (entry 1UMM). According to the data in the PDB, however, the heme axial ligands of *Me*-Cyt c_L are two His residues (His69 and His112), although Afolabi et al. (*22*) have reported that Met109 is the sixth ligand to the heme iron in the protein. Moreover, the X-ray crystal structure of *P. denitrificans* cytochrome c_{551i} (*Pd*-Cyt c_{551i}), which corresponds to Cyt c_L from *M. extorquens*, has been analyzed like that in the ternary complex containing methylamine dehydrogenase, amicyanin, and cytochrome c_{551i} (*21*, *24*). The structure of *Pd*-Cyt c_{551i} is composed of five α-helices; three central helices envelop a heme group and correspond to analogous helices in many *c*-type cytochromes.

This paper describes the X-ray crystal structures, and kinetic studies of MDH (*Hd*-MDH) and Cyt c_L (*Hd*-Cyt c_L) from a methylotrophic denitrifying bacterium, *Hyphomicrobium denitrificans* A3151.[2] A pair of *Hd*-Cyt c_L monomers is related with a pseudo-2-fold axis of symmetry in the asymmetric unit. The configuration of the coupled *Hd*-Cyt c_L monomers is the first example in the studies of cytochrome *c* as the physiological electron acceptor for MDH. *Hd*-MDH is an $\alpha_2\beta_2$ heterotetramer having a molecular 2-fold axis of symmetry like other type I MDHs (*28*). The kinetic investigations have indicated that these proteins tightly interact with each other at pH 5.5. On the basis of these results, we discuss the interaction between these two proteins.

EXPERIMENTAL PROCEDURES

Purification of Hd-MDH and Hd-Cyt c_L. H. denitrificans A3151 was cultured in a mineral salt medium containing 1% (v/v) methanol and 0.5% (w/v) potassium nitrate at 30 °C for 3 days under static conditions (*29*). The cells suspended in 40 mM Tris-HCl buffer (pH 7.5) containing 0.5 mM phenylmethanesulfonyl fluoride were sonicated at 180 W for 30 min, followed by centrifugation at 15 000 rpm for 1 h at 4 °C. The resulting supernatant was applied directly onto a Super Q-Toyopearl column (5 cm × 15 cm, Tosoh), which had been equilibrated with 40 mM Tris-HCl buffer (pH 7.5), as described in a previous paper (*30*). The brown fraction, which was not adsorbed on the column, was employed for the following *Hd*-MDH purification. *Hd*-Cyt c_L adsorbed on the column was eluted with a linear gradient of 0 to 200 mM NaCl in the same buffer. Ammonium sulfate was added to a final concentration of 45% saturation to the *Hd*-Cyt c_L-containing fractions, and the resulting precipitate was removed by centrifugation. The supernatant was applied onto a phenyl-Sepharose Fast Flow column (2.5 cm × 25 cm, Amersham) preequilibrated with 40 mM Tris-HCl (pH 7.5) containing a 45% saturated concentration of ammonium sulfate. *Hd*-Cyt c_L was eluted with a linear gradient from 45 to 0% saturated concentration of ammonium sulfate in the same buffer. The *Hd*-Cyt c_L-containing fractions were collected and then dialyzed with 20 mM Tris-HCl (pH 7.5) for 12 h. The dialyzed sample was applied onto a Resource Q column (1.6 cm × 3.0 cm, Amersham) preequilibrated with 20 mM Tris-HCl buffer (pH 7.5). The elution of *Hd*-Cyt c_L was performed with a linear gradient of 0 to 240 mM NaCl in 20 mM Tris-HCl (pH 7.5) at a flow rate of 1.0 mL/min. Ammonium sulfate was added to 55% saturation to the collected fractions. After removal of precipitates, the sample was applied onto a Phenyl-5PW column (0.9 cm × 5.0 cm, Tosoh), and then *Hd*-Cyt c_L was eluted with a linear gradient from 55 to 0% saturated concentration of ammonium sulfate. The fractions were collected, concentrated, and desalted with a Centriprep-YM10 device (Millipore).

Steady-State Kinetics. The activities of MDH with *Hd*-Cyt c_L were measured in assay mixtures (0.3 mL) containing

[1] Abbreviations: MDH, methanol dehydrogenase; *Hd*-MDH, methanol dehydrogenase from *H. denitrificans* A3151; *Me*-MDH, methanol dehydrogenase from *M. extorquens* AM1; *Pd*-MDH, methanol dehydrogenase from *P. denitrificans*; Cyt c_L, cytochrome c_L; *Hd*-Cyt c_L, cytochrome c_L from *H. denitrificans* A3151; *Me*-Cyt c_L, cytochrome c_L from *M. extorquens* AM1; *Pd*-Cyt c_{551i}, cytochrome c_{551i} from *P. denitrificans*; *Mb*-Cyt c_6, cytochrome c_6 from *Mo. braunii*; MADH, methylamine dehydrogenase; SDS−PAGE, sodium dodecyl sulfate−polyacrylamide gel electrophoresis; PEG, polyethylene glycol; HEPES, *N*-(2-hydroxyethyl)piperazine-*N*′-2-ethanesulfonic acid; Tris, tris(hydroxymethyl)aminomethane; MES, 2-(*N*-morpholino)ethanesulfonic acid; rms, root-mean-square; NCS, noncrystallographic symmetry; ET, electron transfer.

[2] *H. denitrificans* is not only a methylotrophic bacterium but also a denitrifying bacterium. From this strain, copper-containing nitrite reductase and nitrous oxide reductase involved in denitrification have been isolated by the authors (*25*−*27*).

CH_3OH (400 mM), NH_4Cl (10 mM), and various concentrations of the oxidized *Hd*-Cyt c_L (1, 2, 5, 10, 20, and 50 μM) in 10 mM acetic acid/acetate (pH 4.5 and 5.0), MES-NaOH (pH 5.5, 6.0, and 6.5), and Tris-HCl (pH 7.0) buffers. The reactions were started by adding 0.3 nmol of *Hd*-MDH to the mixture. Initial reaction rates were measured by monitoring the increasing absorbance at 550 nm; the absorption coefficients at 550 nm are 25.6 and 7.5 mM^{-1} cm^{-1} for the reduced and oxidized forms of *Hd*-Cyt c_L, respectively. Before the kinetic experiments, *Hd*-Cyt c_L was completely oxidized with a small excess of $K_3[Fe(CN)_6]$. Unreacted $K_3[Fe(CN)_6]$ was removed by passing the mixture through a PD-10 gel-filtration column (Amersham) equilibrated with an appropriate buffer. Apparent kinetic parameters for the reduction of *Hd*-Cyt c_L with *Hd*-MDH were determined according to the following schemes. The reaction mechanism of MDH has been defined as ping-pong-type kinetics (*31*):

$$[E] + [S] \leftrightarrows [E\cdot S] \rightarrow [E''\cdot P] \rightarrow [E''] + [P]$$
$$[E''] + [C] \leftrightarrows [E''\cdot C] \rightarrow [E'\cdot C'] \rightarrow [E'] + [C']$$
$$[E'] + [C] \leftrightarrows [E'\cdot C] \rightarrow [E\cdot C'] \rightarrow [E] + [C'] \quad (1)$$

E, E′, and E″ stand for the oxidized, semiquinone, and fully reduced forms of *Hd*-MDH, respectively. S and P are methanol and formaldehyde, respectively. C and C′ stand for the oxidized and reduced forms of *Hd*-Cyt c_L, respectively. The data obtained can be described by a ping-pong kinetic equation for the three reactants (eq 2) (*31*):

$$v = V[S][C]^2[A]/K_S[C]^2[A] + 2K_C[S][C][A] + K_A[S][C]^2 + [S][C]^2[A] \quad (2)$$

A stands for ammonium chloride as an activator, and K_S, K_C, and K_A are the limiting Michaelis constants for methanol, *Hd*-Cyt c_L, and ammonium chloride, respectively. V and v are the limiting maximum rate and the observed reaction rate, respectively. For a fixed ammonia concentration, eq 2 can be arranged to give eq 3:

$$v = V'[S][C]^2/K_S'[C]^2 + 2K_C'[S][C] + [S][C]^2 \quad (3)$$

When a large excess of methanol (400 mM) is added to the reaction mixture, the apparent V' and K_C' are estimated with eq 3.

Stopped-Flow Kinetics. Stopped-flow experiments were carried out at 25 °C with a RA-2000 stopped-flow spectrophotometer (Otsuka Electronics). The reduction of *Hd*-Cyt c_L with *Hd*-MDH was monitored at 550 nm. To determine the kinetic constants, the concentrations of *Hd*-MDH were up to 10-fold greater than that of *Hd*-Cyt c_L. Pseudo-first-order rate constants were calculated by nonlinear regression with a Guggenheim algorithm available with RA-system (Otsuka Electronics) or IgorPro version 4.02 (WaveMetrics). The data obtained were the average of at least three experiments (the errors were normally within 5%). The experiments were carried out by mixing *Hd*-MDH and oxidized *Hd*-Cyt c_L in 10 mM MES buffer adjusted at pH 5.5 and 6.5. The simple kinetic mechanism for the electron transfer reaction, which includes a complex formation step, is given by eq 4, where semiquinone *Hd*-MDH (semi-MDH) and oxidized *Hd*-Cyt c_L (oxi-Cyt c_L) are changed into oxidized *Hd*-MDH (oxi-MDH) and reduced *Hd*-Cyt c_L (red-Cyt c_L), respectively:

$$\text{semi-MDH} + \text{oxi-Cyt } c_L \underset{k_2}{\overset{k_1}{\rightleftarrows}} [\text{semi-MDH}\cdot\text{oxi-Cyt } c_L] \underset{k_4}{\overset{k_3}{\rightleftarrows}} [\text{oxi-MDH}\cdot\text{red-Cyt } c_L] \quad (4)$$

In this scheme, k_3 is the forward rate constant of the electron transfer reaction and k_4 is the rate of the backward reaction. Thus, k_3 corresponds to k_{ET}, and K_d is equal to k_2/k_1. As described by Harris et al. (*15*), the data were analyzed with eq 5:

$$k_{obs} = k_3[MDH]/([MDH] + K_d) + k_4 \quad (5)$$

Crystallization, Data Collection, and Refinement. Both crystals of *Hd*-MDH and *Hd*-Cyt c_L were grown at 16 °C by the hanging-drop vapor diffusion method. For *Hd*-MDH crystallization, a 1 μL aliquot of protein [20 mg/mL in 40 mM Tris-HCl buffer (pH 7.5)] was mixed with an equal volume of precipitant consisting of 0.2 M potassium thiocyanate and 20% PEG 3350. In the case of *Hd*-Cyt c_L crystallization, 1 μL of 20 mg/mL protein in 20 mM Tris-HCl buffer (pH 7.5) was mixed with an equal volume of the mother solvent containing 2 mM $ZnSO_4$ and 20% PEG 10000 in 100 mM HEPES buffer (pH 7.3). The samples were stored for crystallization in an incubator from 1 week to 1 month at 16 °C.

Diffraction data were independently collected at beamlines BL44XU (for *Hd*-MDH) and BL44B2 (for *Hd*-Cyt c_L) of SPring-8. In the case of the *Hd*-MDH crystal, the X-ray data were collected using a DIP-6040 detector (Bruker-AXS) at 100 K from a single crystal. The crystal belonged to space group *C*2 with the following cell parameters: a = 291.32 Å, b = 63.99 Å, c = 109.94 Å, and β = 105.74°. The intensity data were processed and scaled using HKL2000/SCALEPACK (*32*). The resulting data set contained 68 363 unique reflections with an R_{merge} of 10.2%. A set of reflections representing 10% of the unique data was chosen at random for inclusion in an R_{free} set. The structure of *Hd*-MDH was determined by molecular replacement using MOLREP in the CCP4 suite (*33*, *34*). The molecular structure of *Me*-MDH determined at 1.94 Å (*14*) was used as the search model after first omitting PQQ, Ca^{2+}, water, and the side chains of the amino acid residues, which differ in the two proteins. The resulting initial model gave an *R*-factor of 42% at 2.5 Å resolution after rigid body refinement. On the basis of this model, an electron density map was used for fitting the omitted side chains to generate the start model for refinement. NCS restraints were employed with CNS (*35*) during the early refinement of the *Hd*-MDH model, and then the model was manually rebuilt and adjusted by using XtalView (*36*). The electron densities were subjected to density modification (solvent flattening and histogram matching) performed by DM in the CCP4 suite. At later stages, REFMAC (*37*) was used for refinement without NCS, and solvent molecules were gradually included in the model. Only solvent molecules with thermal parameters lower than 60 $Å^2$ and a reasonable hydrogen bonding environment were included in the final model.

The X-ray data of the *Hd*-Cyt c_L crystal were collected using an ADSC Q-210 detector at 100 K. The crystal

Table 1: Data Collection and Refinement Statistics

	Hd-MDH	*Hd*-Cyt c_L
crystallographic data		
wavelength (Å)/beamline	0.9/BL44XU	0.7/BL44B2
space group	*C*2	$P2_1$
unit cell parameters	$a = 291.32$ Å, $b = 63.99$ Å, $c = 109.94$ Å, $\beta = 105.74°$	$a = 45.78$ Å, $b = 57.28$ Å, $c = 67.01$ Å, $\beta = 101.55°$
resolution range (Å)	35.5−2.50	29.2−1.98
total no. of observations	609090	196240
no. of unique reflections	68363	23538
completeness (%)	99.9 (99.9)[a]	99.6 (99.8)[a]
R_{merge} (%)[b]	10.2 (49.0)[a]	8.2 (43.8)[a]
$I/\sigma(I)$[c]	12.5 (3.2)[a]	15.9 (3.1)[a]
refinement statistics		
R_{cryst}[d]	0.173 (0.256)[a]	0.185 (0.214)[a]
R_{free}[e]	0.234 (0.325)[a]	0.191 (0.223)[a]
no. of amino acid residues	2003	336
no. of non-H protein atoms	15748	2584
no. of heme *c* molecules	−	2
no. of PQQ molecules	3	−
no. of Ca atoms	3	−
no. of solvent molecules	834	456
B values (Å^2)		
protein	38.2	22.0
PQQ and Ca	63.2	−
heme *c*	−	14.9
water	31.9	36.2
rms deviations		
bond lengths (Å)	0.006	0.019
bond angles (deg)	1.4	1.9
Ramachandran plot		
most favored region (%)	83.1	90.3
additional and generously allowed regions (%)	16.4	9.7

[a] The values in parentheses are for the highest-resolution shell: 2.59−2.50 Å for *Hd*-MDH and 2.03−1.98 Å for *Hd*-Cyt c_L. [b] $R_{merge} = \sum_h\sum_i|I(h) - I_i(h)|/\sum_h\sum_i I_i(h)$, where $I_i(h)$ and $I(h)$ are the *i*th and mean measurements of reflection *h*. [c] $\langle I/\sigma(I)\rangle$ is the average signal-to-noise ratio for merged reflection intensities. [d] $R_{cryst} = \sum_h|F_o - F_c|/\sum_h|F_o|$, where F_o and F_c are the observed and calculated structure factor amplitudes, respectively, of reflection *h*. [e] R_{free} is for the test reflection data set, ∼10% selected randomly for cross-validation during the crystallographic refinement.

belonged to space group $P2_1$ with the following unit cell parameters: $a = 45.78$ Å, $b = 57.28$ Å, $c = 67.01$ Å, and $\beta = 101.55°$. Integration and data scaling were carried out using HKL2000/SCALEPACK, and the data set was 99.6% complete overall to 1.98 Å resolution with an R_{merge} of 8.2%. The method of molecular replacement was applied; the molecule of *Pd*-Cyt c_{551i} from the MADH−amicyanin−*Pd*-Cyt c_{551i} complex (PDB entry 2MTA) was used as the model chosen for solving the rotation and translation in MOLREP. Rigid body and simulated annealing refinements and other crystallographic calculations were carried out using CNS and REFMAC in the CCP4 suite. The Zn^{2+} ions added to the mother solvent for the crystallization were observed in the interface between *Hd*-Cyt c_L molecules related with crystallographic symmetry along with a 2-fold spiral axis. Ten Zn^{2+} ions are coordinated to Glu3-A, His106-A, Asp109-A, Asp138-A, Glu153-A, Glu3-B, Glu52-B, Glu53-B, Glu134-B, Glu153-B, Lys157-B, and several water molecules. Both data collection and refinement statistics of *Hd*-MDH and *Hd*-Cyt c_L are summarized in Table 1.

Complex Modeling of Hd-MDH and Hd-Cyt c_L. The MDH−Cyt c_L docking procedure is similar to the method used by Smith and Sternberg (*38*, *39*). First, FTDOCK (*40*) was used to create a set of candidate complex structures. The monomer structure of *Hd*-Cyt c_L (*Hd*-Cyt c_L-A) and the $\alpha_2\beta_2$ heterotetrameric structure of *Hd*-MDH were employed as search models for the docking simulation. The default values for the grid step (0.7 Å) and rotation step (12°) were used. The complementarities of both the interacting surfaces and simple electrostatic criteria were used to generate a set of 10 000 candidate complexes. As the second stage, the first stage of reassessment was performed with RPSCORE (*41*); the observed contacts between different amino acid residues in the complex were scored according to statistical potentials derived from the likelihood of the contacts in a database of protein−protein complexes taken from SCOP 1.53 (http://scop.mrc-lmb.com.ac.uk/scop/). The possible 50 models were selected for the next step.

The electron transfer process is known to be strongly dependent on the distance between the electron donor and acceptor groups (PQQ and heme *c* in the *Hd*-MDH−*Hd*-Cyt c_L complex) (*42*). For this reason, we used the distance between the redox active sites in the next selection step (*43*, *44*). The distance from the sixth ligand (Met103) of the heme in *Hd*-Cyt c_L to Cys103 or Cys104 of *Hd*-MDH (the characteristic disulfide on the PQQ ring) was calculated. The complex models, in which at least one of the distances is less than 21 Å, were selected. By the use of these selected models, the second half of *Hd*-Cyt c_L in the model was generated by utilizing the 2-fold symmetry of the *Hd*-MDH molecule.

RESULTS AND DISCUSSION

Characterization of Hd-Cyt c_L and Hd-MDH. Two soluble cytochrome *c* species are isolated from *H. denitrificans* A3151. An electron acceptor of reduced *Hd*-MDH, *Hd*-Cyt c_L, is an acidic protein (19 kDa) bound to an anion exchange column, while another cytochrome *c* passed through the column, cytochrome c_{550} (*Hd*-Cyt c_{550}), is a basic protein of 10 kDa. The latter corresponds to Cyt c_H from methylotrophic bacteria (*5*, *11*) and is a physiological electron donor for the cognate Cu-containing nitrite reductase (*25*). *Hd*-Cyt c_L has a midpoint redox potential (E_m) of 210 mV (vs NHE) at pH 7.0. The electronic absorption spectrum of reduced *Hd*-Cyt c_L shows five peaks at 280.6 nm ($\epsilon = 39.7$ M^{-1} cm^{-1}), 316.5 nm ($\epsilon = 33.4$ M^{-1} cm^{-1}), 416.2 nm ($\epsilon = 144$ M^{-1} cm^{-1}), 522.0 nm ($\epsilon = 15.9$ M^{-1} cm^{-1}), and 550.7 nm ($\epsilon = 25.6$ M^{-1} cm^{-1}), and that of the oxidized form exhibits four peaks at 281.4 nm ($\epsilon = 36.6$ M^{-1} cm^{-1}), 359.0 nm ($\epsilon = 28.0$ M^{-1} cm^{-1}), 409.3 nm ($\epsilon = 109$ M^{-1} cm^{-1}), and 528.7 nm ($\epsilon = 10.6$ M^{-1} cm^{-1}). In the oxidized form, the near-infrared band at 695 nm was observed, suggesting the presence of the Met-(S^δ)−Fe bond. *Hd*-Cyt c_L has a low-spin heme in both forms.

Compared with those in MDHs from methylotrophs, the Ca^{2+} ion in *Hd*-MDH is easily depleted from the active center by treatment with ammonium sulfate during enzyme preparation (*30*). *Hd*-MDH without the ammonium sulfate treatment in this study contains ∼1.43 Ca^{2+} atoms and two semiquinone PQQ groups per heterotetramer ($\alpha_2\beta_2$); the molecular masses of the α- and β-subunits are 65 and 9 kDa, respectively. The general properties [molecular masses, electronic absorption spectrum, EPR spectrum, and amino acid sequence (*30*)] of *Hd*-MDH are quite similar to those of MDHs from methylotrophs (*10*, *45*−*48*).

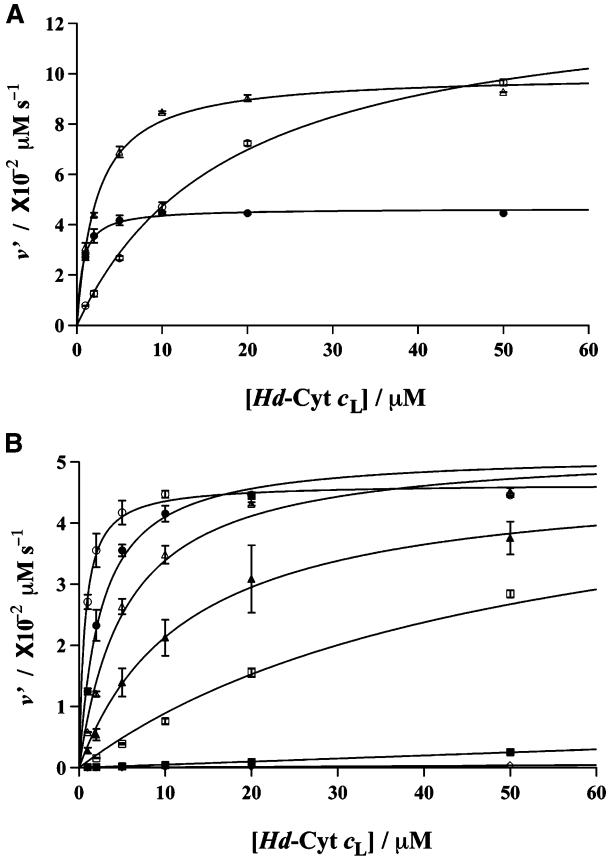

FIGURE 1: Plots of MDH activity (v') vs *Hd*-Cyt c_L concentration ([*Hd*-Cyt c_L]) in the absence (A) and presence (B) of NaCl: (A) pH 4.5 (○), 5.5 (●), and 6.5 (△). (B) The NaCl concentrations in the reaction mixtures at pH 5.5 are 0 (○), 12.5 (●), 25 (△), 50 (▲), 100 (□), 500 (■), and 1000 mM (◇).

Steady-State Kinetics. To investigate the affinity between *Hd*-MDH and *Hd*-Cyt c_L, the dependence of *Hd*-Cyt c_L concentration on MDH activity at various pH values (4.5, 5.0, 5.5, 6.0, 6.5, and 7.0) was measured under steady-state conditions. In Figure 1A, the MDH activity (v') is plotted as a function of *Hd*-Cyt c_L concentration at pH 4.5, 5.5, and 6.5. The plot of v' versus *Hd*-Cyt c_L concentration at pH 5.5 shows obviously that the v' immediately reaches the maximum rate (V') at the low concentration of *Hd*-Cyt c_L. The steady-state kinetic parameters at various pH values are represented in Table 2. It is noteworthy that K_C' (0.3 μM) for *Hd*-Cyt c_L at pH 5.5 is the smallest; that is, *Hd*-Cyt c_L clearly shows the highest affinity for *Hd*-MDH at this pH value. The values of V' are increased under more acidic and basic conditions than pH 5.5, although the affinity of *Hd*-Cyt c_L is decreased. The activity of *Hd*-MDH seems to be maintained at pH 4.5−9.0, but the affinity of *Hd*-Cyt c_L is considerably affected by the pH values. To evaluate the important factors for the interaction between *Hd*-MDH and *Hd*-Cyt c_L, we further investigated the ionic strength dependency of the K_C' values at pH 5.5. The curves of the plot of v' versus *Hd*-Cyt c_L concentration monotonically decline along with NaCl concentration (0−1.0 M) and no longer exhibit the curved profiles in the presence of more than 500 mM NaCl (Figure 1B). These results clearly indicate that the electrostatic interactions are essential for the interaction between *Hd*-MDH and *Hd*-Cyt c_L. The K_C' values under various concentrations of NaCl were estimated to be 1.3 ± 0.1 μM (12.5 mM NaCl), 2.7 ± 0.3 μM (25 mM NaCl), 6.2 ± 1.2 μM (50 mM NaCl), and 24.9 ± 2.9 μM (100 mM NaCl). Interestingly, the ionic strength dependency of the K_C' values was observed not only at high ionic strengths but also at low ionic strengths below ~0.1 M. In the low-ionic strength range, it has been defined by van Leeuwen theory that the observed dependency is dominated not by the dipole moments of each molecules but by the monopole−monopole interaction (*15*). This tendency seems to be inconsistent with the interaction between *Pd*-MDH and *Pd*-Cyt c_{551i} (*15*) but to be similar to that between *Me*-MDH and *Me*-Cyt c_L (*12*). Because the most important factor involved in monopole−monopole interaction is the net charges of molecules (*15*), we attempted to estimate the net charges of MDH (α- and β-subunits) and Cyt c_L from three bacteria, *H. denitrificans*, *P. denitrificans*, and *M. extorquens* AM1. In these proteins, it was assumed that all Glu and Asp residues are deprotonated, all Lys residues are protonated, all Arg residues are in monopositive forms, the terminal amino and carboxyl groups are protonated and deprotonated, respectively, and half of the His residues are protonated. For Cyt c_L, it was assumed that the propionic side chains of the heme moiety are deprotonated and the charge of the iron(III) coordination sphere is +1. For MDH, the charges associated with the carboxyl groups of the PQQ prosthetic group and Ca^{2+} were included. According to these data, the net charges for *Hd*-MDH α- and β-subunits and *Hd*-Cyt c_L were calculated to be −8.5, 5.5, and −8.0, respectively. The charges of *Pd*-MDH, *Pd*-Cyt c_{551i}, *Me*-MDH, and *Me*-Cyt c_L were also estimated to −19.5 (*Pd*-MDH α-subunit), −2.5 (*Pd*-MDH β-subunit), −18.0 (*Pd*-Cyt c_{551i}), −4.0 (*Me*-MDH α-subunit), 5.5 (*Me*-MDH β-subunit), and −5.0 (*Me*-Cyt c_L). As expected, the charges of *Hd*-MDH and *Hd*-Cyt c_L are quite similar to those of *Me*-MDH and *Me*-Cyt c_L but are different from those of *Pd*-MDH and *Pd*-Cyt c_{551i}. The number of Lys residues in *Pd*-Cyt c_{551i} is only five, and *Pd*-MDH has many of the acidic residues (Glu and Asp) compared to *Hd*- and *Me*-MDHs; therefore, the total net charges of *Pd*-MDH and *Pd*-Cyt c_{551i} are extremely more negative than those of

Table 2: Steady-State Kinetic Parameters of MDH Activity with *Hd*-Cyt c_L

pH [I^a (M)]	$K_C'^b$ (μM)	V' ($\times 10^{-2}$ μM s^{-1})	specific activity (μmol min^{-1} mg^{-1})	k_{cat}' (s^{-1})	k_{cat}'/K_C' ($\times 10^{-2}$ μM^{-1} s^{-1})
4.5 (0.0168)	9.0 (0.5)^c	13.3 (0.3)^c	0.36 (0.01)^c	0.45 (0.01)^c	5.0
5.0 (0.0181)	2.6 (0.3)^c	12.2 (0.4)^c	0.33 (0.01)^c	0.41 (0.01)^c	15.8
5.5 (0.0160)	0.3 (0.1)^c	4.6 (0.1)^c	0.12 (0.01)^c	0.15 (0.01)^c	50.0
6.0 (0.0172)	0.6 (0.1)^c	6.3 (0.2)^c	0.17 (0.01)^c	0.21 (0.01)^c	35.0
6.5 (0.0183)	1.1 (0.1)^c	10.0 (0.1)^c	0.27 (0.01)^c	0.33 (0.01)^c	30.0
7.0 (0.0198)	10.5 (1.1)^c	26.1 (1.0)^c	0.70 (0.03)^c	0.87 (0.03)^c	8.3

[a] Ionic strengths in the reaction mixture at each pH value were estimated with the equation $I = ([\text{buffer}] + [Na^+] + [Cl^-] + [NH_4^+])/2$. [b] K_C' values were defined as the limiting Michaelis constant for *Hd*-Cyt c_L. [c] Values in parentheses are errors.

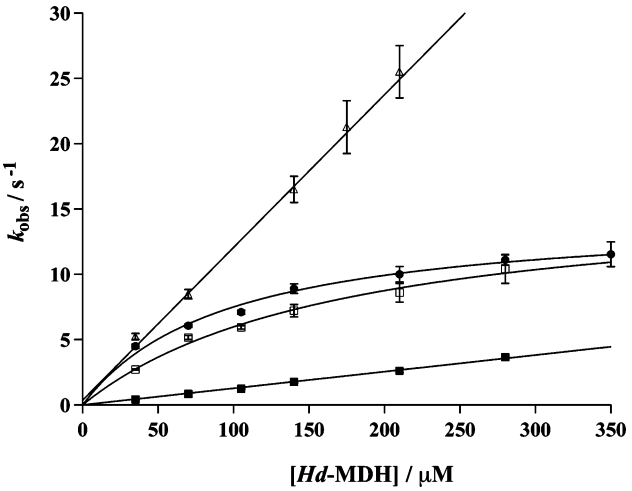

FIGURE 2: Dependence of the observed reduction rate constant (k_{obs}) of *Hd*-Cyt c_L on *Hd*-MDH concentration ([*Hd*-MDH]) at pH 5.5 (●), 6.5 (△), and 5.5 in the presence of 12.5 (□) and 50 mM NaCl (■).

Hd- and *Me*-MDHs and the corresponding cytochrome c_L species. As the optimum pH for the affinity between *Hd*-MDH and *Hd*-Cyt c_L from steady-state kinetics is pH 5.5 (Table 2), we again attempted to calculate the charges of *Hd*-MDH and *Hd*-Cyt c_L at the pH value. The resulting charges were −0.9 (*Hd*-MDH α-subunit), 6.8 (*Hd*-MDH β-subunit), and −6.0 (*Hd*-Cyt c_L), and the total *Hd*-MDH ($\alpha_2\beta_2$) charge is 11.8, which is complementary with the negative charge of *Hd*-Cyt c_L. Therefore, it is suggested that the net charge is one of the important factors for the interaction between *Hd*-MDH and *Hd*-Cyt c_L.

Stopped-Flow Kinetics. The k_{obs} values (eq 5) were obtained under conditions that included a definite *Hd*-Cyt c_L concentration of 3.5 μM and a different *Hd*-MDH concentration between 35 and 350 μM at pH 5.5 and 6.5. The reduction of *Hd*-Cyt c_L is monophasic and obeys pseudo-first-order kinetics. However, the slope of the plot of k_{obs} versus *Hd*-MDH concentration at pH 5.5 is different from that at pH 6.5 (Figure 2). At pH 6.5, no limiting value of k_{obs} was obtained within the range of *Hd*-MDH concentrations. From the slope, the bimolecular rate constant was determined to be 1.2×10^5 M^{-1} s^{-1}. This value is almost comparable to that of *Hyphomicrobium* X previously reported (2.1×10^5 M^{-1} s^{-1} at pH 7.0) (*9*). On the other hand, the slope of the k_{obs} plots at pH 5.5 shows a hyperbolic dependence with respect to *Hd*-MDH concentration. This saturation effect provides unambiguous evidence for a process involving an initial binding step that equilibrates much faster than the following electron transfer step (eq 4). Therefore, these findings imply formation of a transient complex between *Hd*-MDH and *Hd*-Cyt c_L, when the electron transfer reaction occurs at the interface between these proteins. The *y*-intercept of the k_{obs} plots passes through the origin in Figure 2, indicating that k_4 is essentially zero (*15*); consequently, the kinetic parameters k_{ET} and K_d for the reduction of *Hd*-Cyt c_L with *Hd*-MDH were determined to be 14.6 ± 0.7 s^{-1} and 95 ± 12 μM, respectively. Like the K_C' values from steady-state kinetics, the K_d value is also affected dramatically by ionic strength at pH 5.5. The slope of the plot of k_{obs} no longer shows a hyperbolic curve profile in the presence of 50 mM NaCl (Figure 2), being obviously lower than that at pH 6.5. The resulting bimolecular rate constant was determined to be 1.3×10^4 M^{-1} s^{-1}. Interestingly, the resulting slope of the k_{obs} plot at pH 5.5 in the presence of 12.5 mM NaCl shows a hyperbolic profile like that at pH 5.5 in the absence of NaCl (Figure 2), although the K_C' value (1.1 ± 0.1 μM) at pH 6.5 is comparable to the value of 1.3 ± 0.1 μM at pH 5.5 in the presence of 12.5 mM NaCl. These findings clearly indicate that the difference in the slopes of the k_{obs} plots at pH 5.5 (hyperbolic) and 6.5 (linear) is not due to the difference in the association constants at the same pH values. Therefore, we should consider a more complex electron transfer reaction model for understanding the electron transfer reaction between these proteins. According to the kinetic complexity (Scheme 1) determined by Davidson (*21*), it is suggested that the rate (k_{ET}) of the ET process is accelerated and/or the equilibrium constant (K_X) of the non-ET process is increased by the pH change from 5.5 to 6.5 in the electron transfer reaction between *Hd*-MDH and *Hd*-Cyt c_L.

Scheme 1: Kinetic Complexity Model (*21*)

$$A_{ox} + B_{red} \underset{}{\overset{K_a}{\rightleftarrows}} A_{ox} - B_{red} \underset{k_{-X}}{\overset{k_X}{\rightleftarrows}} [A_{ox} - B_{red}]^* \underset{k_{-ET}}{\overset{k_{ET}}{\rightleftarrows}} A_{red} - B_{ox}$$

true ET:	$k_{ET} \ll k_X$	$K_X (k_X/k_{-X}) \gg 1$	$k_{obs} = k_{ET}$
gated ET:	$k_X \ll k_{ET}$		$k_{obs} = k_X$
coupled ET:	$k_{ET} \ll k_X$	$K_X(k_X/k_{-X}) \ll 1$	$k_{obs} = K_X k_{ET}$

If the electron transfer reaction between *Hd*-MDH and *Hd*-Cyt c_L at pH 5.5 is "coupled ET" like that between *Pd*-MDH and *Pd*-Cyt c_{551i} (*15*), the unfavorable non-ET process might become more favorable at pH 6.5. Alternatively, if the electron transfer reaction is "gated ET" or "true ET", k_X or k_{ET} will be increased. Therefore, it is likely that the pH change from 5.5 to 6.5 accelerates dramatically the rate of the electron transfer reaction (non-ET process and/or ET process), although the affinity between *Hd*-MDH and *Hd*-Cyt c_L becomes weak (Table 2).

Crystal Structures of Hd-Cyt c_L and Hd-MDH. The crystal structure of *Hd*-Cyt c_L was determined at 1.98 Å resolution. The final values of *R* and R_{free} are 0.18 and 0.19, respectively, and the rms deviations of bond lengths and angles from ideal values are 0.019 Å and 1.9°, respectively. The crystal belongs to space group $P2_1$ and contains two monomer molecules of *Hd*-Cyt c_L in the asymmetric unit. Each monomer is composed of a polypeptide containing 168 amino acid residues and one *c*-type heme group covalently bound to Cys59 and Cys62 (Figure 3A). There are a total of 11 helices in the monomer structure, as determined by the Database of Secondary Structure of Proteins [DSSP (*49*)]; the five central helices (α3, α4, η2, α5, and α6) envelop the heme group. The axial ligands of the heme group are His63 and Met103, although those of *Me*-Cyt c_L have been registered as two His residues in the Protein Data Bank (entry 1UMM). The conformation of the axial Met103 ligand of *Hd*-Cyt c_L is significantly similar with the model proposed by NMR (*50*); that is, the Met103 S^δ atom in *Hd*-Cyt c_L has the S configuration, and the lone pair electrons are directed toward the nitrogen of pyrrole B of the heme group (Figure 3B). Three torsion angles are −175.2° ($N-C^\alpha-C^\beta-C^\gamma$), 51.2° ($C^\alpha-C^\beta-C^\gamma-S^\delta$), and −162.2° ($C^\beta-C^\gamma-S^\delta-C^\epsilon$). The imi-

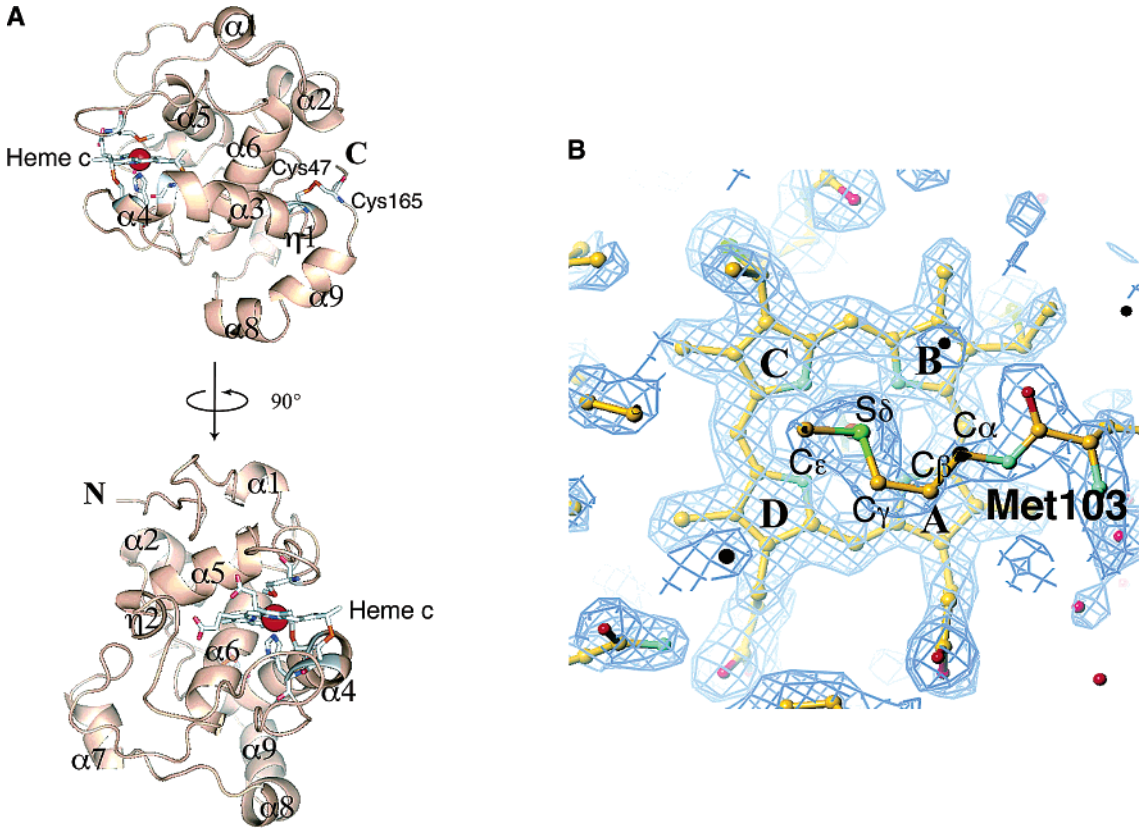

FIGURE 3: Structures of *Hd*-Cyt c_L and the axial Met103 ligand at 2.0 Å resolution. (A) Ribbon diagram of *Hd*-Cyt c_L with a heme *c* group, the axial ligands, covalently bound Cys, and the intramolecular disulfide bond shown in stick presentation. The Fe atom of the heme group is represented by a red sphere. (B) The $2F_o - F_c$ electron density map (contoured at 1σ) of Met103 and heme *c*.

dazole plane orientation of the His63 ligand is aligned with the heme *meso* protons at positions 5 and 15. Moreover, there is an intramolecular disulfide bond between Cys47 and Cys165 (Figure 3A). The C-terminal region (Ile125−Ser168) is linked to the core region (Ala45−His124) by this bridge, which looks like a fixer of the flexible α8 and α9 helices in the C-terminal region.

Two *Hd*-Cyt c_L molecules (*Hd*-Cyt c_L-A and -B) having a pseudo-2-fold axis of symmetry in the asymmetric unit are interacted with each other (pattern I), as shown in Figure 4A. In pattern I, there are three hydrogen bonds: Lys31-A N^{ζ}−Glu23-B $O^{\epsilon}2$ (2.88 Å), Asp26-A $O^{\delta}2$−Gly24-B N (2.68 Å), and Gly24-A N−Asp26-B $O^{\delta}2$ (3.28 Å). It should be noted that these amino acid residues are included in the N-terminal region (Ala1−Val44) of *Hd*-Cyt c_L. Moreover, it was also found that there is a different interaction with another molecule in the neighborhood of the asymmetric unit (pattern II) (Figure 4B). Pattern II shows no direct interaction between *Hd*-Cyt c_L-A and -B, and the gap between the two molecules is occupied with several water molecules. The distances between Fe atoms of *Hd*-Cyt c_L-A and -B are 53.7 Å in pattern I and 19.6 Å in pattern II. Additionally, the remarkable structural difference between *Hd*-Cyt c_L-A and -B was also observed. In *Hd*-Cyt c_L-B, helix α7 containing the region of Val130−Pro146 is displaced from that in *Hd*-Cyt c_L-A by ca. 50° (Figure 4B).

The structure of *Hd*-Cyt c_L was compared with those of the other cytochrome *c* species in the Protein Data Bank with DALI (*51*). Two proteins with the highest *Z* score are *Pd*-Cyt c_{551i} from the MADH−amicyanin−*Pd*-Cyt c_{551i} crystalline complex (PDB entry 2MTA, $Z = 24.2$, and rms deviation = 1.3 Å) and cytochrome c_6 (*Mb*-Cyt c_6) from *Monophidium braunii* (PDB entry 1CTJ, $Z = 8.2$, and rms deviation = 1.9 Å). As expected from a level of amino acid sequence homology of 48% between *Hd*-Cyt c_L and *Pd*-Cyt c_{551i}, the X-ray structure analyses of these proteins show a strong resemblance in the backbone structures (Figure 5A). However, the existence of the disulfide bond of the C-terminal region (Lys148−Ser155) in *Pd*-Cyt c_{551i} is unknown, because the coordinates of its region have not been reported (*24*). The C-terminal structure of *Hd*-Cyt c_L, which contains the disulfide bridge, is uniquely characteristic. In Figure 5B, the structure of *Mb*-Cyt c_6 is significantly similar to that of *Hd*-Cyt c_L in the core region only, although the level of amino acid sequence homology between the core regions (total of 89 residues of *Mb*-Cyt c_6) of these proteins exhibits a relatively low value (17.8%). Moreover, the cytochrome *c* domain (Pro577−His664) of quinohemoprotein alcohol dehydrogenase [ADH IIB (*28*), PDB entry 1KV9] was also used for a structural comparison with *Hd*-Cyt c_L. The core folding of *Hd*-Cyt c_L is similar to that of the cytochrome *c* domain in ADH IIB, while the N- and C-terminal regions of the former are obviously different from the corresponding regions of the latter; no terminal regions exist in the cytochrome *c* domain of ADH IIB (Figure 5C). The level of amino acid sequence homology between its cytochrome *c* domain and the core region of *Hd*-Cyt c_L is low (19%). It is concluded that the core region of *Hd*-Cyt c_L has a common folding fashion conserved in many cytochrome *c* structures, but the unique N- and C-terminal regions are conserved only in a unique physiological electron acceptor for type I MDH, Cyt c_L. Therefore, these regions are presumed to play

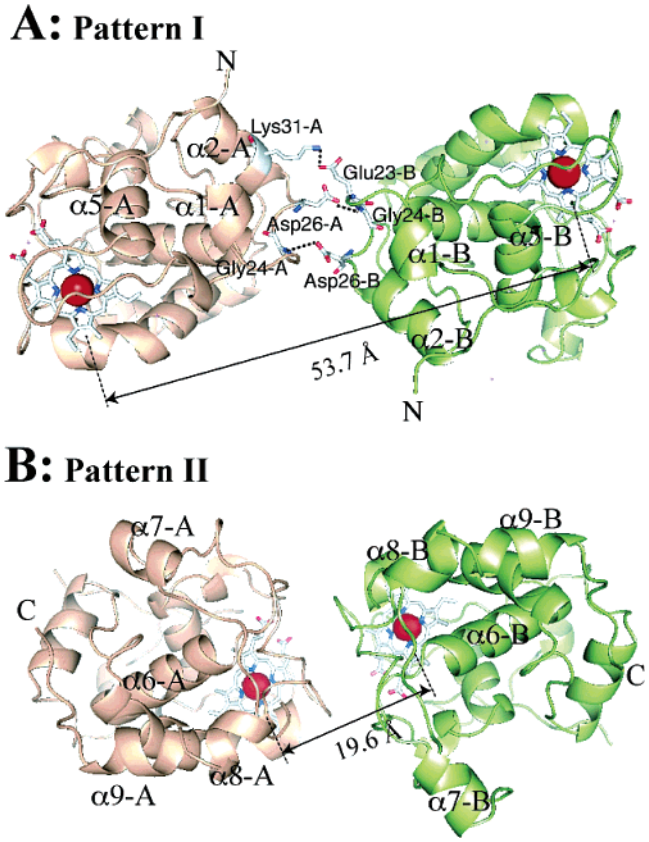

FIGURE 4: Orientation and interaction between two *Hd*-Cyt c_L monomers in the asymmetric unit. (A) In the pattern I configuration, the amino acid residues involved in the direct interaction between two *Hd*-Cyt c_L monomers and the heme group are shown in stick representation. *Hd*-Cyt c_L-A and -B are colored wheat and lime, respectively. (B) Pattern II configuration.

important roles in the interaction with MDH during the electron transfer process.

The crystal structure of *Hd*-MDH was determined at 2.5 Å resolution. The *Hd*-MDH crystal belongs to space group *C*2 and contains one heterotetramer ($\alpha_2\beta_2$) and one heterodimer ($\alpha\beta$) in the asymmetric unit. The latter forms a heterotetramer structure with another heterodimer molecule related with crystallographic symmetry. The overall structure of *Hd*-MDH shows a striking resemblance (rms deviations for the Cα atoms of ~0.4 Å) to the other MDH structures (*17*−*20*), which is consistent with the fact that the amino acid sequence of *Hd*-MDH is remarkably similar to those of the other MDHs (60−80%) (*30*). The common structural characteristics of MDH are also conserved in *Hd*-MDH: the numbers and positions of disulfide bridges, amino acid residues in the cis configuration, and the "tryptophan docking motif". Panels A and B of Figure 6 depict the surface electrostatic potential and ribbon diagram of heterotetrameric *Hd*-MDH, respectively. The basic β-subunit (Figure 6B, colored lime) is composed of 72 amino acid residues containing 13 Lys and 3 Arg residues. Acidic *Hd*-Cyt c_L has a negative potential around the hydrophobic patch-centered heme. Therefore, the accessible surface of *Hd*-MDH is dominated by positive electrostatic potential, which is distributed near the β-subunit.

Structural and Mechanistic Insights into Interactions between Hd-Cyt c_L and Hd-MDH. The interaction between *Pd*-MDH and *Pd*-Cyt c_{551i} has recently been investigated by

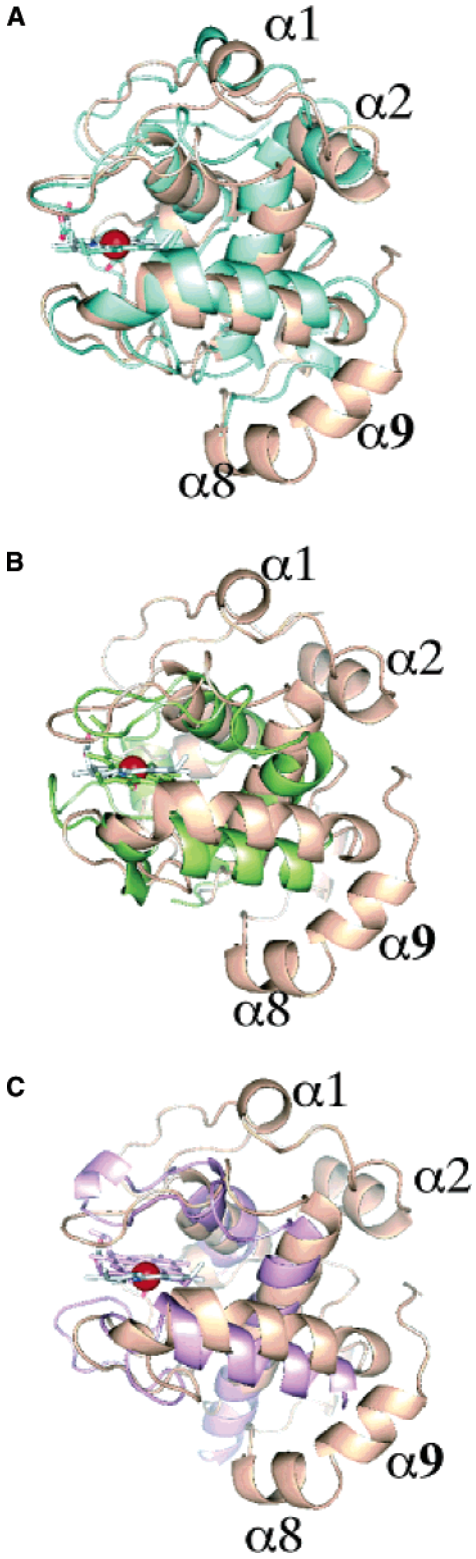

FIGURE 5: Structural comparison of *Hd*-Cyt c_L with three cytochrome *c* species: (A) vs *Pd*-Cyt c_{551i}, (B) vs *Mb*-Cyt c_6, and (C) vs the Cyt *c* domain of ADH IIB. *Hd*-Cyt c_L, *Pd*-Cyt c_{551i}, *Mb*-Cyt c_6, and the Cyt *c* domain of ADH IIB are colored wheat, cyan, lime, and pink, respectively.

molecular modeling using the X-ray coordinates of those proteins (*20*). The most attractive models were obtained during manual modeling with the two Cyt *c* molecules permitted to bind to the MDH heterotetramer at the same time. It was suggested that the binding of the second Cyt *c* would be a more efficient process, when one site has already

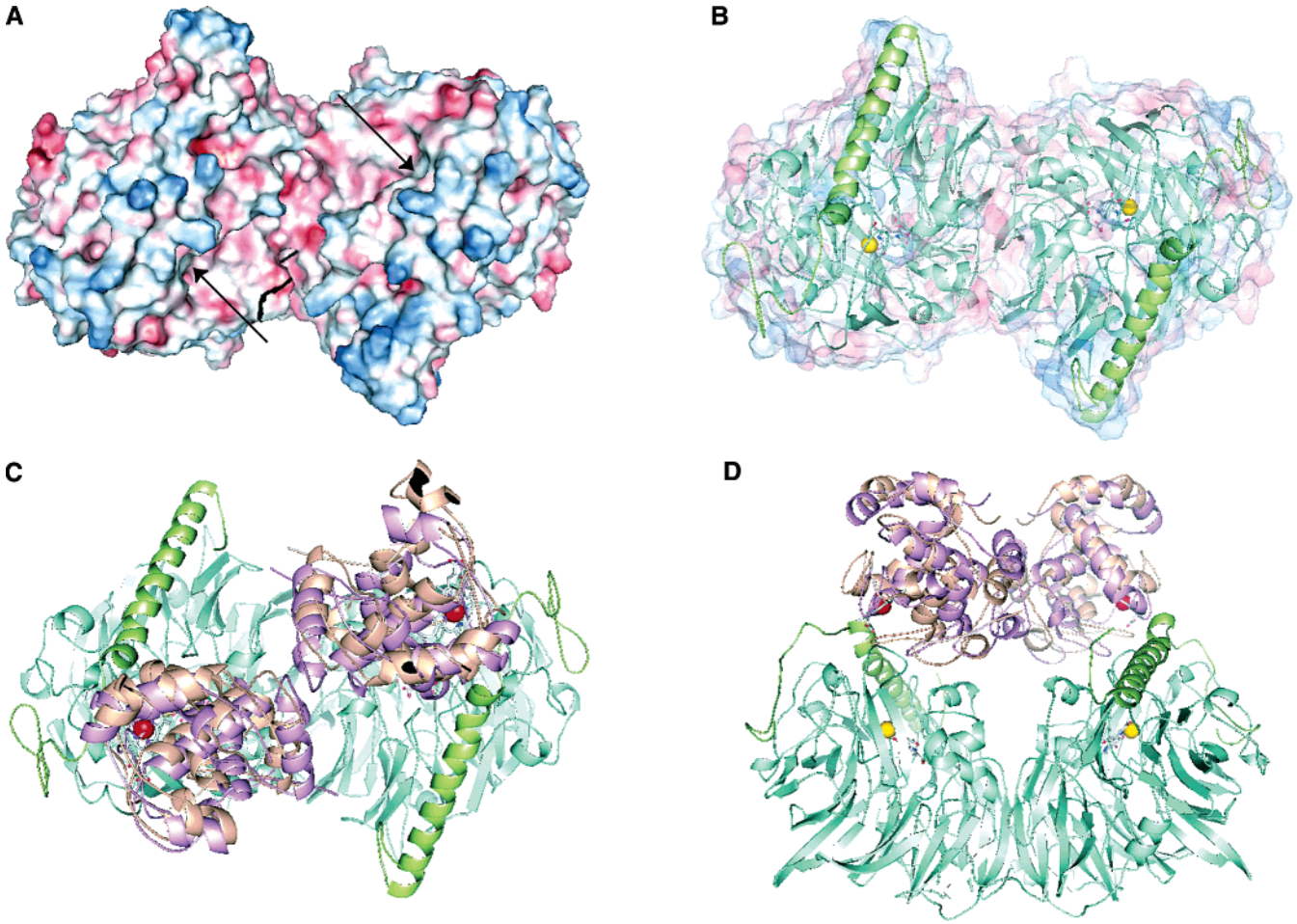

FIGURE 6: Surface electrostatic potential of *Hd*-MDH and docking model between *Hd*-MDH and *Hd*-Cyt c_L. (A) Surface electrostatic potential of the *Hd*-MDH ($\alpha_2\beta_2$) molecule. Blue and red denote positive and negative potentials, respectively, and white represents neutral area. Arrows indicate the PQQ site at the bottom of the solvent-accessible cleft on the protein surface of *Hd*-MDH. (B) Ribbon diagram of the *Hd*-MDH molecule overlaid with the surface electrostatic potential shown in panel A. The α- and β-subunits are colored cyan and lime, respectively. Ca^{2+} in the active center is represented as a yellow sphere. (C) Possible model of docking for *Hd*-MDH and *Hd*-Cyt c_L. Two *Hd*-Cyt c_L molecules (pink) in the complex model (RPSCORE ID of 23) calculated with FT-DOCK and two *Hd*-Cyt c_L monomers (wheat) are related by 2-fold axis symmetry by the present X-ray structure analysis. (D) Rotation (90°) of the model complex shown in panel C. The Fe atom of the heme group in *Hd*-Cyt c_L is represented as a red sphere.

been occupied. However, the previous kinetic studies of the reaction of *Pd*-MDH with *Pd*-Cyt c_{551i} provided no evidence of cooperativity (*15*, *16*). In the study of the crystal structure of *Hd*-Cyt c_L presented here, we found that two *Hd*-Cyt c_L molecules related by a 2-fold axis in the asymmetric unit interact with each other. This finding is the first example of the unique configuration of Cyt c_L as a physiological electron acceptor for MDH and would be important for the interaction with MDH from the perspective that the $\alpha_2\beta_2$ heterotetrameric structure of the enzyme also has a 2-fold axis of symmetry. Therefore, we further investigated whether it is possible to keep the configuration of two *Hd*-Cyt c_L molecules during the formation of a complex with *Hd*-MDH by using FTDOCK for protein−protein docking simulation. The *Hd*-Cyt c_L monomer and *Hd*-MDH heterotetramer molecules were employed for the calculation. After docking and scoring, we obtained several candidates. The possible model complexes were selected by filtering on the basis of the PQQ−heme distance and by eliminating the models in which a "docked" Cyt c_L molecule collides with the rotated one, when the complex is rotated on a molecular 2-fold axis of heterotetrameric *Hd*-MDH docking one Cyt c_L molecule. When one of the candidates (RPSCORE ID of 23) is rotated on a molecular 2-fold axis of *Hd*-MDH, the configuration of the docked *Hd*-Cyt c_L molecules is almost consistent with the pattern I configuration observed in the crystal structure (Figure 6C,D). Furthermore, it has been confirmed that *Hd*-Cyt c_L dimerizes with itself in solution, because of the formation of the cross-linked species with a mass of ~40 kDa (Figure 7, left). These facts strongly suggest that this unique configuration of *Hd*-Cyt c_L perhaps has an important meaning in terms of the interaction with *Hd*-MDH.

The newly proposed docking model with *Hd*-MDH and *Hd*-Cyt c_L in this study was analyzed by comparing with quinohemoprotein alcohol dehydrogenase ADH IIB (PDB entry 1KV9) and the proposed docking models between *Pd*-MDH and *Pd*-Cyt c_{551i} (*20*). The α-subunit of *Hd*-MDH shows a high degree of structural similarity with the quinone domain of ADH IIB, while no β-subunit exists in ADH IIB (Figure 8). The function of the β-subunit remains unknown in the previous MDH studies, but it is strongly suggested in this study that the *Hd*-MDH β-subunit plays an important role in the effective interaction with *Hd*-Cyt c_L by controling the total net charge of *Hd*-MDH and the surface electrostatic potential near the PQQ active center (Figure 6A,B). This suggestion is also supported by the FTDOCK docking

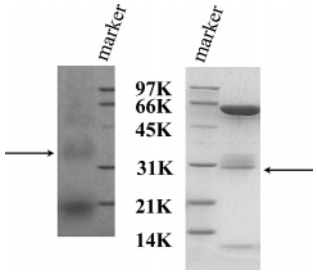

FIGURE 7: SDS−PAGE of the cross-linked species. The left panel shows SDS−PAGE of the cross-linked *Hd*-Cyt c_L dimer. *Hd*-Cyt c_L (60 μg) was added to 30 μL of 10 mM Mes buffer (pH 5.5) containing 4 mM 1-ethyl-3-[3-(dimethylamino)propyl]carbodiimide (EDC) and 10 mM *N*-hydroxysuccinimide (NHS). After the mixture was incubated at 30 °C for 30 min, the sample was applied to the gel (12 μg). The arrow indicates the *Hd*-Cyt c_L dimer (~40 kDa). The right panel shows SDS−PAGE of the cross-linked *Hd*-MDH−Cyt c_L complex. *Hd*-Cyt c_L was activated with the cross-linking reagents EDC and NHS at pH 6.5. After desalting had been carried out, the activated *Hd*-Cyt c_L (final concentration of 10 μM) was added to 10 mM Mes buffer (pH 5.5) containing 100 μM *Hd*-MDH and then was incubated at 25 °C for 160 min. Ammonium acetate (10 mM) was added finally to the mixture, and the resulting complex was purified chromatographically. The fraction containing the *Hd*-MDH−Cyt c_L complex was applied to the gel (5 μg). The arrow indicates the cross-linked β-subunit−*Hd*-Cyt c_L monomer complex (28 kDa; 9 kDa β-subunit and 19 kDa Cyt c_L).

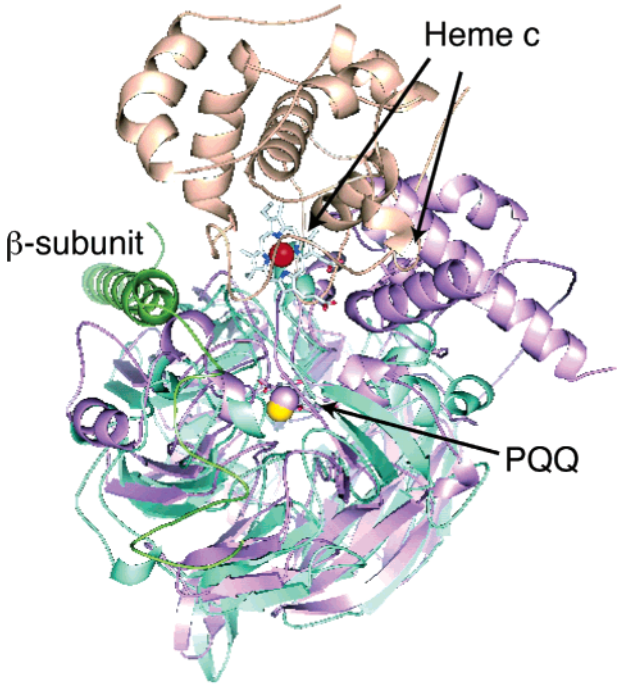

FIGURE 8: Structural comparison of the *Hd*-MDH−*Hd*-Cyt c_L docking model and ADH IIB. The α-subunit of *Hd*-MDH was superimposed on the quinone domain of ADH IIB: α-subunit (cyan) and β-subunit (lime) of *Hd*-MDH, *Hd*-Cyt c_L (wheat), and ADH IIB (pink).

simulation, which proposed that the binding position of *Hd*-Cyt c_L in *Hd*-MDH seems to be more stable at the site near the β-subunit than the Cyt *c* domain in ADH IIB having no β-subunit (Figure 8). Moreover, the interaction between the β-subunit and *Hd*-Cyt c_L was also confirmed by a cross-linking study, which shows the cross-linked species with a mass of ~30 kDa [*Hd*-MDH β-subunit (9 kDa) + *Hd*-Cyt c_L (19 kDa)] on SDS−PAGE (Figure 7, right). The four salt bridges are proposed in the interface between *Hd*-MDH and *Hd*-Cyt c_L: αArg426···Asp109-A, βLys35···Glu57-A, βAsp33···Lys70-A, and βLys31···Glu68-A. This interaction means it is predominantly electrostatic and is consistent with the results of the ionic strength dependence in steady-state and stopped-flow kinetics (Figures 1B and 2). The shortest distance between the PQQ and heme in this model was estimated to 18.2 Å, ~4 Å longer than that between the PQQ and heme in ADH IIB (~14 Å). Therefore, the proposed model of the *Hd*-MDH−*Hd*-Cyt c_L complex appears to be similar to the proposed ionic "docking complex" of *Me*-MDH with *Me*-Cyt c_L (*12*); that is, the ionic strength dependence observed in the *Hd*-MDH−*Hd*-Cyt c_L complex is quite similar to that of of the *Me*-MDH−*Me*-Cyt c_L complex. Salts inhibit the initial complex formation process, and not the subsequent electron transfer process. Moreover, the initial docked Cyt c_L is suggested to move to its optimal position for the electron transfer process, probably involving an interaction with the hydrophobic funnel on the surface of MDH.

On the other hand, the proposed model of the *Pd*-MDH−*Pd*-Cyt c_{551i} complex is assigned as an electron transfer complex model using the coordinates of ADH IIB, in which the two proteins have been located at the optimum position for the electron transfer (*20*). It is slightly different from the *Hd*-MDH−*Hd*-Cyt c_L docking model. The proposed position of *Pd*-Cyt c_{551i} seems to be rotated in the counterclockwise direction by ~90° compared to the orientation of *Hd*-Cyt c_L in the *Hd*-MDH−*Hd*-Cyt c_L docking model and to be slightly far from the β-subunit compared to the position of *Hd*-Cyt c_L. This observation might be true, because the *Hd*-MDH−*Hd*-Cyt c_L docking model is in the initial docking state, while the proposed model of the *Pd*-MDH−*Pd*-Cyt c_{551i} complex is in the electron transfer state. Therefore, it is suggested that the difference between these docking models may implicate the activation mechanism on the non-ET process for the electron transfer reaction between MDH and Cyt c_L; the mechanism implies that the interaction between the two proteins changes from the initial docking site to the optimal site for the electron transfer. Alternatively, the difference might be due to the character of MDHs, because *Pd*-MDH has a more strongly negative net charge than *Hd*-MDH and its electron transfer reaction was observed even under high-ionic strength conditions (≤3.0 M NaCl) (*15*), although no electron transfer occurs in the *Hd*-MDH−*Hd*-Cyt c_L complex.

In this study, the catalytic efficiency and formation of a transient complex of *Hd*-MDH with *Hd*-Cyt c_L show an optimum pH of 5.5, and *Hd*-Cyt c_L is proposed to dimerize transiently during the initial electrostatic binding process with *Hd*-MDH. Although the overall reaction mechanism of *Hd*-MDH is defined as simple ping-pong-type kinetics at present, the real mechanism might be more complexed, because *Hd*-MDH exhibits a heterotetrameric structure ($\alpha_2\beta_2$) and has two independent active centers per molecule and two Cyt c_L molecules bind to the two active centers at same time and/or stepwise. If the binding constant and the electron transfer rate constant of the first Cyt c_L obviously distinguish it from the second Cyt c_L under steady-state kinetic conditions, the simple kinetics model (in eqs 1−3) should be reconsidered. However, they have not been determined in the previous MDH−Cyt c_L studies. Therefore, at present, we could only assume that the binding constant and the

electron transfer rate of the first Cyt c_L are equal to those of the second Cyt c_L. An attempt to determine pK_a values of amino acid residues involved in formation of the complex was carried out by analyzing the slope of log k_{cat}'/K_C' plots. However, it was difficult to determine their precise values because of few observed plots and the complicated interactions between the two proteins. At pH 4.5−7.0, the amino acid residues, which participate in the complex formation by acid dissociation, are Glu and Asp having pK_a values of 4.0−4.5. The protonation/deprotonation of their carboxyl groups on the molecular surface is suggested to be very critical for the docking mechanism and an efficient electron transfer process. Moreover, *Hd*-MDH and *Hd*-Cyt c_L are acidic proteins at neutral pH (*30*); especially *Hd*-Cyt c_L containing a total of 25 acidic amino acid residues on the protein surface is strongly acidic. As shown in Table 2, the pH change from pH 7.0 to 5.5 causes an increase in the affinity between *Hd*-MDH and *Hd*-Cyt c_L because of a decrease in the strength of the repulsion between these acidic proteins by the negative charge loss of the protein surfaces, as proposed in the case of *Pd*-MDH and *Pd*-c_{551i} (*15*).

ACKNOWLEDGMENT

We gratefully acknowledge the staff for assistance in the collection of X-ray data on the RIKEN beamline (BL44B2) and Drs. A. Nakagawa, M. Suzuki, and M. Yoshimura for assistance in the collection of X-ray data on beamline BL44XU at SPring-8 (C05A44XU-7218-N).

REFERENCES

1. Anthony, C. (2004) The quinoprotein dehydrogenases for methanol and glucose, *Arch. Biochem. Biophys. 428*, 2−9.
2. Anthony, C., and Williams, P. (2003) The structure and mechanism of methanol dehydrogenase, *Biochim. Biophys. Acta 1647*, 18−23.
3. Anthony, C. (1996) Quinoprotein-catalyzed reactions, *Biochem. J. 320*, 697−711.
4. Anthony, C. (1993) Methanol dehydrogenase in Gram-negative bacteria, in *Principles and Applications of Quinoproteins* (Davidson, V. L., Ed.) pp 17−45, Marcel Dekker, New York.
5. Anthony, C. (1993) The role of quinoproteins in bacterial energy transduction, in *Principles and Applications of Quinoproteins* (Davidson, V. L., Ed.) pp 223−244, Marcel Dekker, New York.
6. Dijkstra, M., Frank, J. J., van Wielink, J. E., and Duine, J. A. (1988) The soluble cytochromes *c* of methanol-grown *Hyphomicrobium* X: Evidence against the involvement of autoreduction in electron-acceptor functioning of cytochrome c_L, *Biochem. J. 251*, 467−474.
7. Frank, J., and Duine, J. A. (1990) Cytochrome c_L and cytochrome c_H from *Hyphomicrobium* X, *Methods Enzymol. 188*, 303−308.
8. Day, D. J., and Anthony, C. (1990) Soluble cytochromes *c* of methanol-utilizing bacteria, *Methods Enzymol. 188*, 298−303.
9. Dijkstra, M., Frank, J. J., and Duine, J. A. (1989) Studies on electron transfer from methanol dehydrogenase to cytochrome c_L, both purified from *Hyphomicrobium* X, *Biochem. J. 257*, 87−94.
10. Frank, J. J., Dijkstra, M., Duine, J. A., and Balny, C. (1988) Kinetic and spectral studies on the redox forms of methanol dehydrogenase from *Hyphomicrobium* X, *Eur. J. Biochem. 174*, 331−338.
11. Read, J., Gill, R., Dales, S. L., Cooper, J. B., Wood, S. P., and Anthony, C. (1999) The molecular structure of an unusual cytochrome c_2 determined at 2.0 Å; the cytochrome c_H from *Methylobacterium extorquens*, *Protein Sci. 8*, 1232−1240.
12. Dales, S. L., and Anthony, C. (1995) The interaction of methanol dehydrogenase and its cytochrome electron acceptor, *Biochem. J. 312*, 261−265.
13. Chan, H. T. C., and Anthony, C. (1991) The interaction of methanol dehydrogenase and cytochrome c_L in the acidophilic methylotroph *Acetobacter methanolicus*, *Biochem. J. 280*, 139−146.
14. Ghosh, M., Anthony, C., Harlos, K., Goodwin, M. G., and Blake, C. (1995) The refined structure of the quinoprotein methanol dehydrogenase from *Methylobacterium extorquens* at 1.94 Å, *Structure 15*, 177−187.
15. Harris, T. K., Davidson, V. L., Chen, L. F., Mathews, F. S., and Xia, Z.-x. (1994) Ionic strength dependence of the reaction between methanol dehydrogenase and cytochrome *c*-55li: Evidence of conformationally coupled electron transfer, *Biochemistry 33*, 12600−12608.
16. Harris, T. K., and Davidson, V. L. (1993) Binding and electron-transfer reactions between methanol dehydrogenase and its physiologic electron acceptor cytochrome *c*-551i: A kinetic and thermodynamic analysis, *Biochemistry 32*, 14145−14150.
17. Williams, P. A., Coates, L., Mohammed, F., Gill, R., Erskine, P. T., Coker, A., Wood, S. P., Anthony, C., and Cooper, J. B. (2005) The atomic resolution structure of methanol dehydrogenase from *Methylobacterium extorquens*, *Acta Crystallogr. D61*, 75−79.
18. Xia, Z.-X., Dai, W.-W., Zhang, Y.-F., White, S. A., Boyd, G. D., and Mathews, F. S. (1996) Determination of the gene sequence and the three-dimensional structure at 2.4 Å resolution of methanol dehydrogenase from *Methylophilus* W3A1, *J. Mol. Biol. 259*, 480−501.
19. Xia, Z.-X., He, Y.-N., Dai, W.-W., White, S. A., Boyd, G. D., and Mathews, F. S. (1999) Detailed active site configuration of a new crystal form of methanol dehydrogenase from *Methylophilus* W3Al at 1.9 Å resolution, *Biochemistry 38*, 1214−1220.
20. Xia, Z.-X., Dai, W.-W., He, Y.-N., White, S. A., Mathews, F. S., and Davidson, V. L. (2003) X-ray structure of methanol dehydrogenase from *Paracoccus denitrificans* and molecular modeling of its interactions with cytochrome *c*-55li, *J. Biol. Inorg. Chem. 8*, 843−854.
21. Davidson, V. L. (2004) Electron transfer in quinoprotems, *Arch. Biochem. Biophys. 428*, 32−40.
22. Afolabi, P. R., Mohammed, F., Amaratunga, K., Majekodunmi, O., Dales, S. L., Gill, R., Thompson, D., Cooper, J. B., Wood, S. P., Goodwin, P. M., and Anthony, C. (2001) Site-directed mutagenesis and X-ray crystallography of the PQQ-containing quinoprotein methanol dehydrogenase and its electron acceptor, cytochrome c_L, *Biochemistry 40*, 9799−9809.
23. Turano, P., and Lu, Y. (2001) Iron in heme and related proteins, in *Handbook on metalloproteins* (Bertini, I., Sigel, A., and Sigel, H., Eds.) pp 269−356, Marcel Dekker, New York.
24. Chen, L., Durley, R. C. E., Mathews, F. S., and Davidson, V. L. (1994) Structure of an electron transfer complex: Methylamine dehydrogenase, amicyanin, and cytochrome c_{551i}, *Science 264*, 86−90.
25. Deligeer, Fukunaga, R., Kataoka, K., Yamaguchi, K., Kobayashi, K., Tagawa, S., and Suzuki, S. (2002) Spectroscopic and functional characterization of Cu-containing nitrite reductase from *Hyphomicrobium denitrificans* A3151, *J. Inorg. Biochem. 91*, 132−138.
26. Yamaguchi, K., Kataoka, K., Kobayashi, M., Itoh, K., Fukui, A., and Suzuki, S. (2004) Characterization of two type 1 Cu sites of *Hyphomicrobium denitrificans* nitrite reductase: A new class of copper-containing nitrite reductase, *Biochemistry 43*, 14180−14188.
27. Yamaguchi, K., Kawamura, A., Ogawa, H., and Suzuki, S. (2003) Characterization of nitrous oxide reductase from a methylotrophic denitrifying bacterium, *Hyphomicrobium denitrificans*, *J. Biochem. 134*, 853−858.
28. Toyama, H., Mathews, F. S., Adachi, O., and Matsushita, K. (2004) Quinohemoprotein alcohol dehydrogenases: Structure, function, and physiology, *Arch. Biochem. Biophys. 428*, 10−21.
29. Aida, T., and Nomoto, K. (1988) Nitrate removal from a sewage by supplementation of methanol using a submerged soil column, and changes in the population of methanol-utilizing denitrifiers in the column soil, *Jpn. J. Soil Sci. Plant Nutr. 59*, 464−470.
30. Nojiri, M., Hira, D., Yamaguchi, K., Okajima, T., Tanizawa, K., and Suzuki, S. (2005) Preparation and characterization of Ca^{2+}-free methanol dehydrogenase from *Hyphomicrobium denitrificans* A3151, *Chem. Lett. 34*, 1036−1037.
31. Duine, J. A., and Frank, J., Jr. (1980) Studies on methanol dehydrogenase from *Hyphomicrobium* X, *Biochem. J. 187*, 213−219.
32. Otwinnowski, Z., and Minor, W. (1997) Processing of X-ray diffraction data collected in oscillation mode, *Methods Enzymol. 276*, 307−326.
33. Vagin, A. A. (1997) MOLREP: An automated program for molecular replacement, *J. Appl. Crystallogr. 10*, 1022−1025.

34. Potterton, E., Briggs, P., Turkerburg, M., and Dodson, E. (2003) A graphical user interface to the CCP4 program suite, *Acta Crystallogr. D59*, 1131−1137.
35. Brunger, A. T., Adams, P. D., Clore, G. M., DeLano, W. N., Gross, M., Pannu, N. S., Read, R. J., Rice, L. M., Simonson, T., and Warren, G. L. (1998) Crystallography & NMR system: A new software suite for macromolecular structure determination, *Acta Crystallogr. D54*, 905−921.
36. McRee, D. E. (1999) XtalView/Xfit: A versatile program for manipulating atomic coordinates and electron density, *J. Struct. Biol. 125*, 156−165.
37. Murshudov, G. N., Vagin, A. A., and Dodson, E. D. (1997) Refinement of macromolecular structures by the maximum-likelihood method, *Acta Crystallogr. D53*, 240−255.
38. Smith, G. R., and Sternberg, M. J. E. (2002) Prediction of protein−protein interactions by docking methods, *Curr. Opin. Struct. Biol. 12*, 28−35.
39. Smith, G. R., and Sternberg, M. J. E. (2003) Evaluation of the 3D-Dock protein docking suite in rounds 1 and 2 of the CAPRI blind trial, *Proteins 52*, 74−79.
40. Gabb, H. A., Jackson, R. M., and Sternberg, M. J. E. (1997) Modeling protein docking using shape complementarity, electrostatics and biochemical information, *J. Mol. Biol. 272*, 106−120.
41. Moont, G., Gabb, H. A., and Sternberg, M. J. E. (1999) Use of pair potentials across protein interfaces in screening predicted docked complexes, *Proteins 35*, 364−373.
42. Marcus, R. A., and Sutin, N. (1985) Electron transfers in chemistry and biology, *Biochim. Biophys. Acta 811*, 265−322.
43. Flock, D., and Helms, V. (2002) Protein−protein docking of electron transfer complexes: Cytochrome *c* oxidase and cytochrome *c*, *Proteins 47*, 75−85.
44. Mattila, K., and Haltia, T. (2005) How does nitrous oxide reductase interact with its electron donors? A docking study, *Proteins 59*, 708−722.
45. Ohta, S., Fujita, T., and Tobari, J. (1981) Methanol dehydrogenase of *Methylomonas* J: Purification, crystallization, and some properties, *J. Biochem. 90*, 205−213.
46. Richardson, I. W., and Anthony, C. (1992) Characterization of mutants of the quinoprotein methanol dehydrogenase lacking an essential calcium ion, *Biochem. J. 287*, 709−715.
47. Frank, J., and Duine, J. A. (1990) Methanol dehydrogenase from *Hyphomicrobium* X, *Methods Enzymol. 188*, 202−209.
48. Harris, T. K., and Davidson, V. L. (1994) Replacement of enzyme-bound calcium with strontium alters the kinetic properties of methanol dehydrogenase, *Biochem. J. 300*, 175−182.
49. Kabsch, W., and Sander, C. (1983) Dictionary of protein secondary structure: Pattern recognition of hydrogen-bonded and geometrical features, *Biopolymers 22*, 2577−2637.
50. Costa, H. S., Santos, H., and Turner, D. L. (1994) An unusual conformation of the methionine haem ligand in cytochrome c_L established by two-dimensional ^{1}H NMR, *Eur. J. Biochem. 223*, 783−789.
51. Holm, L., and Sander, C. (1993) Protein structure comparison by alignment of distance matrices, *J. Mol. Biol. 223*, 123−138.

BI051877J